

Supplementary Information

Kinetically Controlled Synthesis of Two-Dimensional Zr/Hf Metal-Organic Framework Nanosheets *via* Modulated Hydrothermal Approach

Zhigang Hu,^a Ezwan Mahmoud Mahdi,^b Yongwu Peng,^a Yuhong Qian,^a Bin Zhang,^a Ning Yan,^a Daqiang Yuan,^c Jin-Chong Tan,^b and Dan Zhao^{*a}

^aDepartment of Chemical & Biomolecular Engineering, National University of Singapore, 4 Engineering Drive 4, 117585, Singapore

^bDepartment of Engineering Science, University of Oxford, Parks Road, Oxford OX1 3PJ, UK

^cState Key Laboratory of Structural Chemistry, Fujian Institute of Research on the Structure of Matter, Chinese Academy of Sciences, Fuzhou, 350002 Fujian, China

*Correspondence and requests for materials should be addressed to D.Z. (E-mail:

chezhao@nus.edu.sg).

Experimental Details

Materials and Methods

All the reagents were obtained from commercial suppliers and used without further purification. Field-emission scanning electron microscopy (FE-SEM) was conducted on a FEI Quanta 600 SEM (20 kV) equipped with an energy dispersive spectrometer (EDS, Oxford Instruments, 80 mm² detector). Samples were treated via Pt sputtering before observation. High-resolution transmission electron microscopy (HR-TEM) was conducted on a JEOL-JEM 3010 TEM. Powder X-ray diffraction (PXRD) patterns were obtained on a Bruker D8 Advance X-ray powder diffractometer equipped with a Cu sealed tube ($\lambda = 1.54178 \text{ \AA}$) at a scan rate of 0.02 deg s^{-1} . Thermogravimetric analysis (TGA) was performed using a Shimadzu DTG-60AH thermal analyzer under a flowing N₂ gas (100 mL min^{-1}) with a heating rate of $10 \text{ }^\circ\text{C min}^{-1}$. Elemental analyses (EA) were performed on Vario MICRO series CHNOS elemental analyzer. Atomic force microscopy (AFM) was carried out by testing samples deposited on silica wafers using tapping mode with a Bruker Dimension Icon atomic force microscope.

Modulated Hydrothermal¹⁻² Synthesis of NUS-8

1,3,5-Benzenetricarboxylic acid (H₃BTB, 2.2 g, 5 mmol) and ZrCl₄ (1.2 g, 5.3 mmol) or HfCl₄ (1.7 g, 5.3 mmol) were mixed in 50 mL of mixed solvent containing deionized (DI) water and acetic acid (AA) (v/v = 3/2) in a 100 mL round flask. The flask was placed in an oil bath and heated under reflux ($\sim 120 \text{ }^\circ\text{C}$) for 20 h to yield NUS-8 as white powder. The product was soaked in anhydrous methanol for 3 days at room temperature, during which time the extract was decanted and fresh methanol was added every day. Then the sample was treated with anhydrous dichloromethane similarly for another 3 days. This process was carried out to wash out residual reagents in the pores. After removal of dichloromethane by decanting, the sample was dried under a dynamic vacuum at $120 \text{ }^\circ\text{C}$ for 24 h to yield the final product (yield: 73% based on the total mass of reactants).

Solvothermal Synthesis of NUS-16

The synthesis of NUS-16(Zr) and NUS-16(Hf) was conducted according to the literature.³ Briefly, H₃BTB (110 mg, 0.25 mmol) and ZrCl₄ (120 mg, 0.50 mmol) or HfCl₄ (190 mg, 0.05 mmol) were dissolved in mixed solvent containing dimethylformamide (DMF) and acetic acid (AA) (v/v = 1:3, 16 mL). The mixture was sealed in a tube, slowly heated to $120 \text{ }^\circ\text{C}$ from room temperature within 8 h, kept at $120 \text{ }^\circ\text{C}$ for 72 h, and then slowly cooled to $30 \text{ }^\circ\text{C}$ within 10 h. The product was collected and soaked in anhydrous methanol for 3 days at room temperature, during which the extract was decanted and fresh methanol was added every day. Then the sample was treated with anhydrous dichloromethane similarly for another 3 days. This process was carried out to wash out residual reagents in the pores. After removal of dichloromethane by decanting, the sample was dried under a dynamic vacuum at $120 \text{ }^\circ\text{C}$ for 24 h to yield the final product (yield: 38% based on Zr).

Synchrotron PXRD Data Collection and Structure Determination

Synchrotron PXRD data of NUS-8 for indexing and structural refinement were collected at 300 K with a 0.01° step size using a large imaging plate Debye-Scherrer camera installed on the BL02B2 beam line at SPring-8, Japan. Samples were loaded into 0.5 mm glass capillaries under ambient conditions for data collection. The incident X-ray was monochromated to 12.4

keV ($\lambda = 0.9998 \text{ \AA}$) with a Si (111) double crystal monochromator.

The determination of NUS-8 structures was based on the 3D single crystal model reported by Sun *et al.*³ Briefly, the matching analyses of PXRD patterns were carried out by LeBail route using EXPO2014 program,⁴ giving cubic $P2_1/m$ space groups with $a = 19.923 \text{ \AA}$ for NUS-8(Zr) (see Table S1 for details).

NH₃ Temperature-Programmed Desorption (TPD) Studies⁵

Temperature-programmed desorption (TPD) profiles of NH₃ from the MOF catalysts were examined using a ChemBET *Pulsar* TPR/TPD (Quantachrome). Briefly, 0.1 g of MOF catalyst was charged into a quartz tube (O.D. = 6 mm, I.D. = 4 mm) and then activated in a helium flow of 100 mL min⁻¹ at 150 °C for 2 h. The sample was subsequently exposed to pure ammonia gas (30 mL min⁻¹) for 30 min and then purged with helium flow (100 mL min⁻¹) at 100 °C for 2 h. The temperature of the sample was increased to 450 °C at a ramping rate of 5 °C min⁻¹, and desorbed ammonia was detected using a TCD detector.

Gas Sorption Measurements

Gas sorption isotherms were measured up to 1 bar using a Micromeritics ASAP 2020 surface area and pore size analyzer. Before the measurements, the sample (~80 mg) was degassed under reduced pressure ($< 10^{-2} \text{ Pa}$) at 150 °C for 10 h. UHP grade gases were used for gas sorption measurements. Oil-free vacuum pumps and oil-free pressure regulators were used to prevent contamination of the samples during the degassing process and isotherm measurement. Pore size distribution data were calculated from the N₂ adsorption isotherms at 77 K based on non-local density functional theory (NLDFT) model in the Micromeritics ASAP 2020 software package (assuming slit pore geometry). Pore size distribution data in mesoporous range (2-40 nm) were calculated from the N₂ desorption isotherms at 77 K based on Barrett-Joyner-Halenda (BJH) model in the Micromeritics ASAP 2020 software package.

Calculation of Isothermic Heat of Adsorption (Q_{st})⁶

The gas adsorption isotherms measured at 273 K and 298 K were firstly fitted to a virial equation (Equation 1). The fitting parameters were then used to calculate the isothermic heat of adsorption (Q_{st}) using Equation 2,

$$\ln P = \ln N + \frac{1}{T} \sum_{i=0}^m a_i N^i + \sum_{i=0}^n b_i N^i \quad (1)$$

$$Q_{st} = -R \sum_{i=0}^m a_i N^i \quad (2)$$

where P is pressure (mmHg), N is adsorbed quantity (mmol g⁻¹), T is temperature (K), R is gas constant (8.314 J K⁻¹ mol⁻¹), a_i and b_i are virial coefficients, m and n represent the number of coefficients required to adequately describe the isotherms (herein, $m = 5$, $n = 2$).

Calculation of Gas Selectivity based on Ideal Adsorption Solution Theory (IAST)⁷

The gas adsorption isotherms were firstly fitted to a dual-site Langmuir-Freundlich (DSLFL) model (Equation 3),

$$q = \frac{q_{sat,A} b_A p^{\alpha_A}}{1 + b_A p^{\alpha_A}} + \frac{q_{sat,B} b_B p^{\alpha_B}}{1 + b_B p^{\alpha_B}} \quad (3)$$

where q is the amount of adsorbed gas (mmol g^{-1}), p is the bulk gas phase pressure (bar), q_{sat} is the saturation amount (mmol g^{-1}), b is the Langmuir-Freundlich parameter ($\text{bar}^{-\alpha}$), α is the Langmuir-Freundlich exponent (dimensionless) for two adsorption sites A and B indicating the presence of weak and strong adsorption sites.

IAST starts from the Raoult's Law type of relationship between fluid and adsorbed phase,

$$P_i = Py_i = P_i^o x_i \quad (4)$$

$$\sum_{i=1}^n x_i = \sum_{i=1}^n \frac{P_i}{P_i^o} = 1 \quad (5)$$

where P_i is partial pressure of component i (bar), P is total pressure (bar), y_i and x_i represent mole fractions of component i in gas and adsorbed phase (dimensionless). P_i^o is equilibrium vapour pressure (bar).

In IAST, P_i^o is defined by relating to spreading pressure π ,

$$\frac{\pi S}{RT} = \int_0^{P_i^o} \frac{q_i(P_i)}{P_i} dP_i = \Pi \text{ (Constant)} \quad (6)$$

where π is spreading pressure, S is specific surface area of adsorbent ($\text{m}^2 \text{g}^{-1}$), R is gas constant ($8.314 \text{ J K}^{-1} \text{ mol}^{-1}$), T is temperature (K), $q_i(P_i)$ is the single component equilibrium obtained from isotherm (mmol g^{-1}).

For a dual-site Langmuir-Freundlich (DSLFL) model, we have an analytical expression for the integral,

$$\int_0^{P_i^o} \frac{q_i(P_i)}{P_i} dP_i = \Pi \text{ (Constant)} = \frac{q_{sat,A}}{\alpha_A} \ln[1 + b_A (P_i^o)^{\alpha_A}] + \frac{q_{sat,B}}{\alpha_B} \ln[1 + b_B (P_i^o)^{\alpha_B}] \quad (7)$$

The isotherm parameters will be known from the previous fitting. For a binary component system the unknowns will be Π , P_1^o , and P_2^o which can be obtained by simultaneously solving Equations 5 and 7.

The adsorbed amount for each component in a mixture is

$$q_i^{mix} = x_i q_T \quad (8)$$

$$\frac{1}{q_T} = \sum_{i=1}^n \frac{x_i}{q_i(P_i^o)} \quad (9)$$

where q_i^{mix} is the adsorbed amount of component i (mmol g^{-1}), q_T is the total adsorbed amount (mmol g^{-1}).

The adsorption selectivities S_{ads} were calculated using Equation 10.

$$S_{ads} = \frac{q_1 / q_2}{p_1 / p_2} \quad (10)$$

In this study, IAST calculations were carried out assuming CO_2/N_2 (15/85) binary mixed gases at 298 K and pressures up to 1 bar to mimic the composition and condition of flue gas for

post-combustion CO₂ capture.

Catalytic Oxidation of Thioethers⁸⁻⁹

The catalytic oxidation reactions were conducted in 20 mL glass vials under vigorous agitation at ambient temperature (25 °C). In general, a desired amount of MOF catalyst was loaded into the glass vial, and a solution containing thioanisole and H₂O₂ in dichloromethane (DCM) was added. The reaction vessel was sealed and stirred at 25 °C. For kinetic studies, 50 μL of supernatant solution was taken out and diluted with 0.5 mL of DMSO-d₆ each time. The thioanisole oxidation products (sulfoxide and sulfone) were analysed by ¹H-NMR.

Recyclability of the catalyst: the oxidation of thioanisole was selected as a probe reaction. At first, 0.17 mmol of thioanisole, 0.49 mmol of H₂O₂, and 0.25×10⁻² mmol of MOF (1.5% mole loading, 15~25 mg) were added into 1 mL of DCM. The mixture was stirred for 1 h at 25 °C. Upon the completion of the reaction, another 0.17 mmol of thioanisole and 0.49 mmol of H₂O₂ were added. After that, the mixture was stirred 1 h at 25 °C again. The process was repeatedly performed for three times.

Characterization of Thermo-Mechanical Properties

Temperature-dependent viscoelasticity measurements were performed using the TA Instruments Q800 Dynamic Mechanical Analyser (DMA). Powder samples were evacuated prior to the experiments at 120 °C for 24 hours in vacuum and ground using mortar and pestle to ensure uniformity. The samples were loaded onto a specially-designed concave bar sample holder (to hold powders and liquids), and weight measurements were taken from the clamps before and after the powder samples were loaded. The typical amount of sample used was ~100 mg per run. The samples were evenly distributed in the sample holder to ensure equal distribution of temperature and dynamic mechanical loadings. The powder-based DMA method employed here is different from conventional tests that required the use of a continuous (bulk) material.¹⁰⁻¹¹

The dynamic experiments were performed at a heating rate of 1 °C min⁻¹ from 35 – 350 °C (dual cantilever multi-frequency DMA mode). The DMA was calibrated to a pair of dual cantilever clamps and fixed to a gauge length of 35 mm. The static force was at 0.1 N with the force track set to 125%. The multi-frequency sweep setting was applied, where the oscillating frequency was cyclically alternated between 2, 10, and 20 Hz as the temperature was increased throughout the experiments. At the end of the experiments, the remaining samples were collected and stored for XRD analyses to check for sample integrity post-dynamic loadings. A blank stainless steel sample holder was subjected to corresponding test conditions, and the results from the blank sample holder test were used as a subtraction background for the tested samples. Our approach involves subtracting the thermo-mechanical response of the sample holder and powder samples from that of the sample holder on its own, resulting in the response of the powder alone, which is then reported in this work.

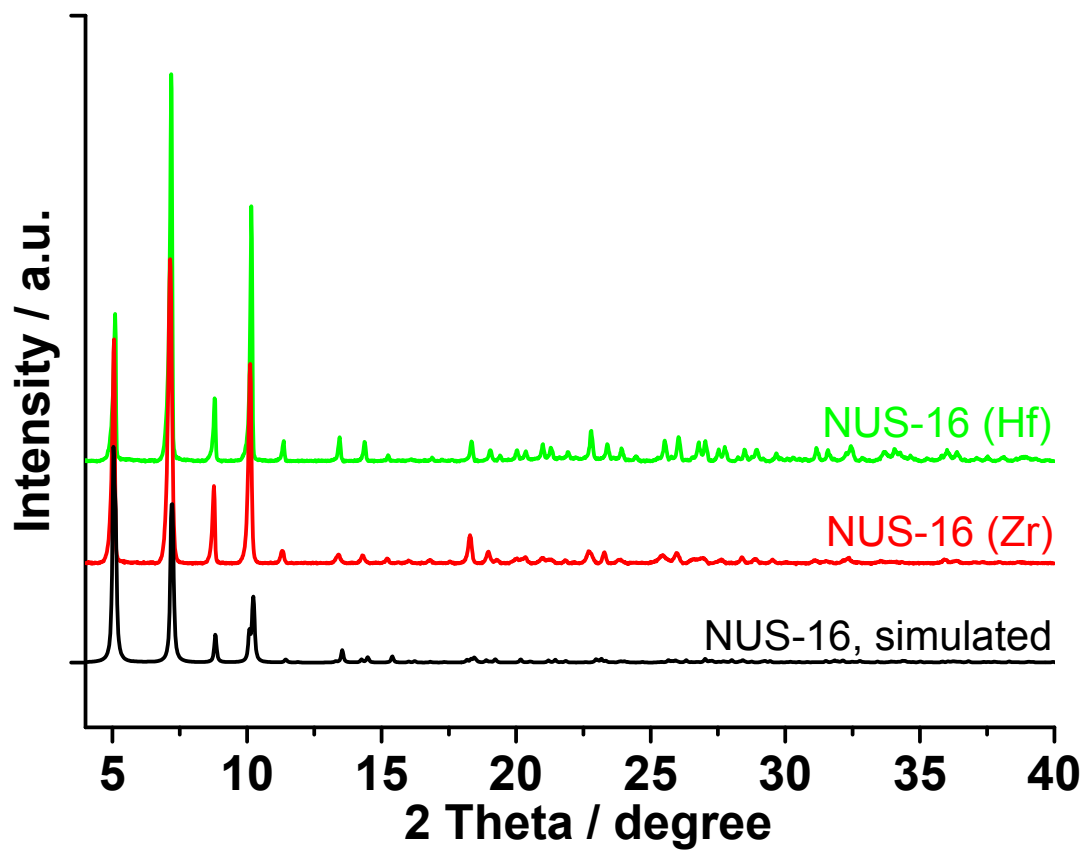


Figure S1. PXRD patterns of calculated and experimental 3D NUS-16 MOFs.

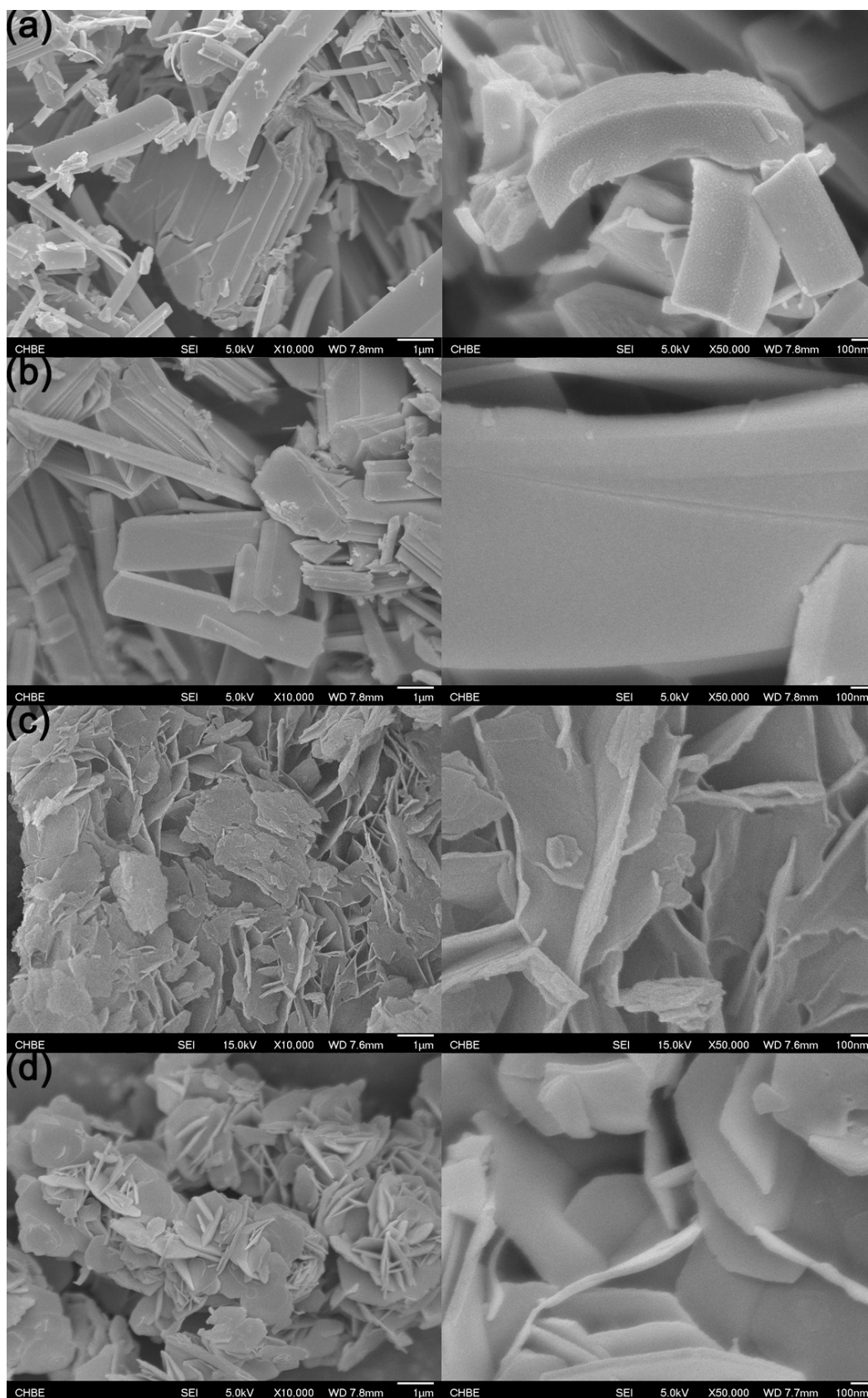


Figure S2. Detailed FE-SEM images: **(a)** NUS-16(Zr). **(b)** NUS-16(Hf). **(c)** NUS-8(Zr). **(d)** NUS-8(Hf).

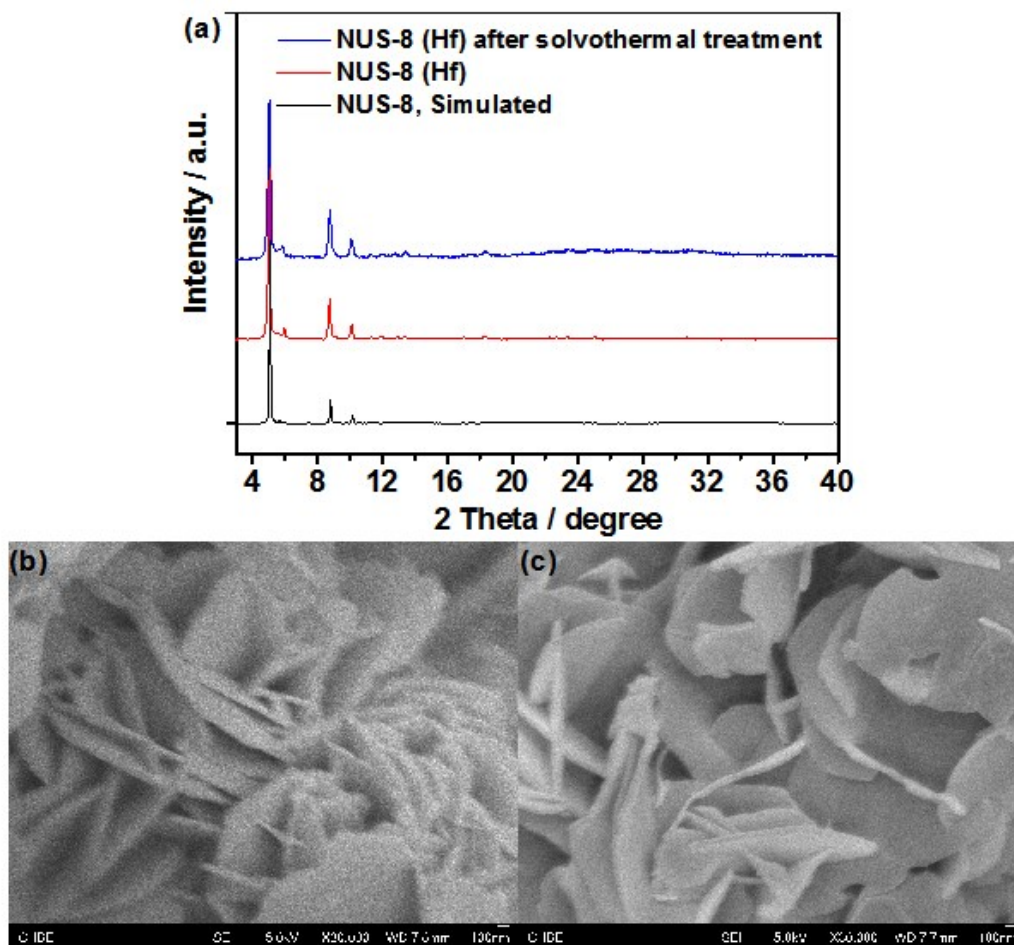


Figure S3. Results of kinetic control experiments using NUS-8(Hf) incubated in DMF/AA solution at 120 °C for 24 h. (a) PXRD patterns; FESEM images of before (b) and after (c) solvothermal treatment.

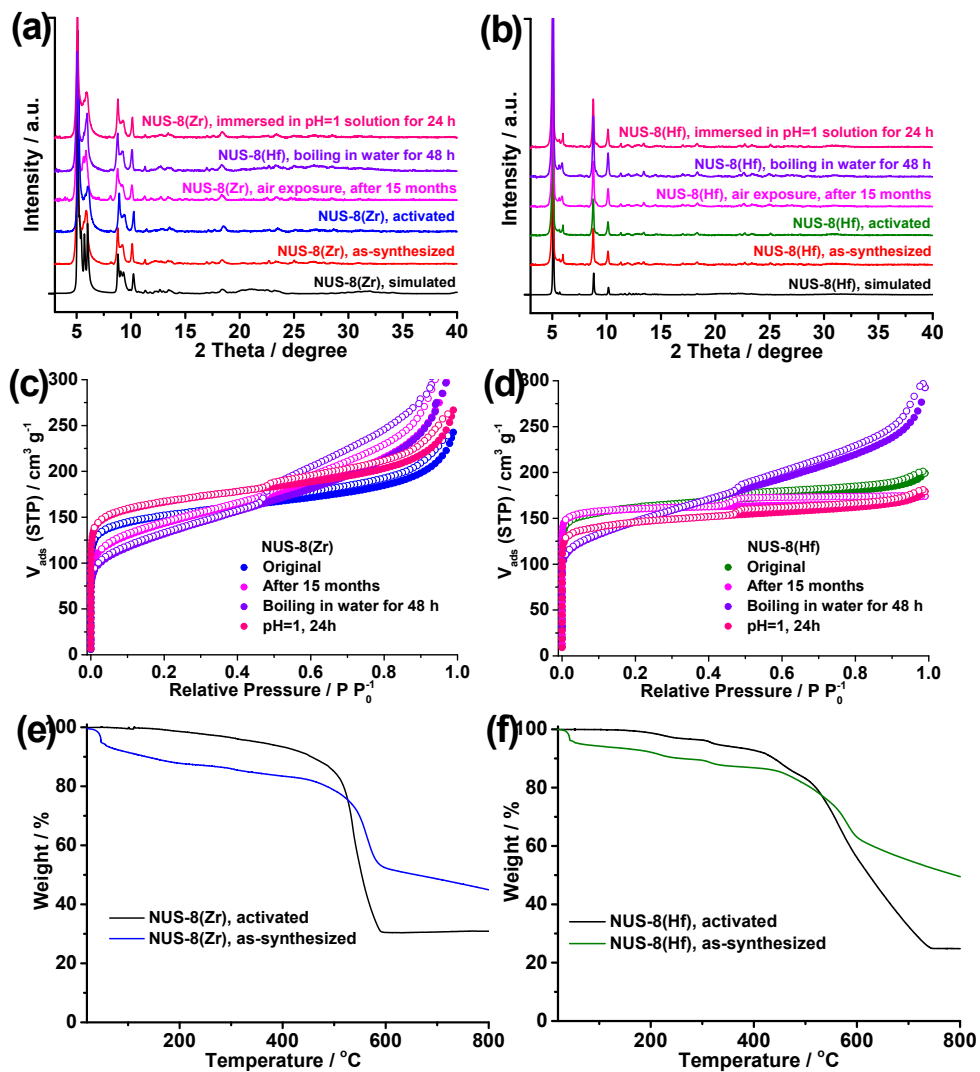


Figure S4. Stability tests of 2D NUS-8 MOFs. (a-b) PXRD patterns; (c-d) N₂ sorption isotherms at 77 K; (e-f) TGA curves. NUS-8(Zr): a, c, e; NUS-8(Hf): b, d, f.

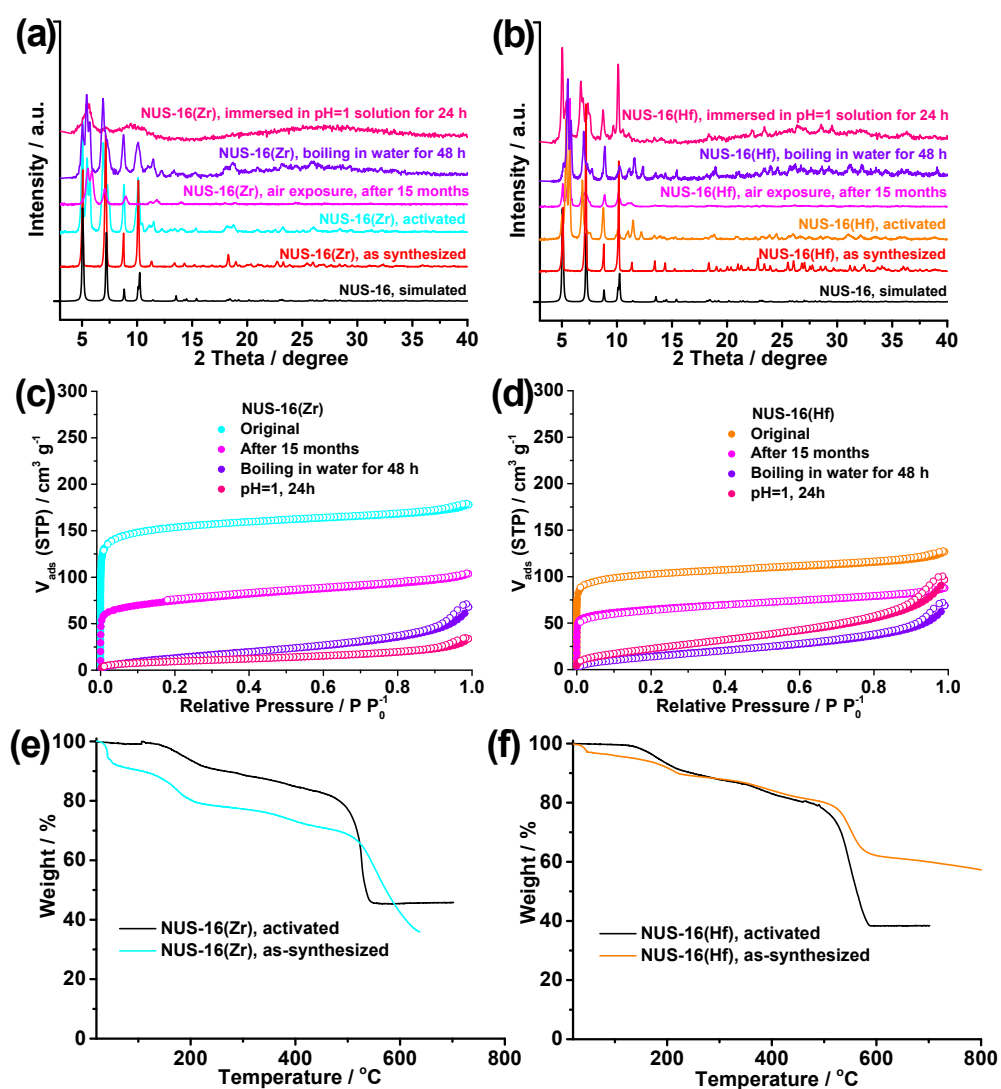


Figure S5. Stability tests of 3D NUS-16 MOFs. (a-b) PXRD patterns; (c-d) N₂ sorption isotherms at 77 K; (e-f) TGA curves. NUS-16(Zr): a, c, e; NUS-16(Hf): b, d, f.

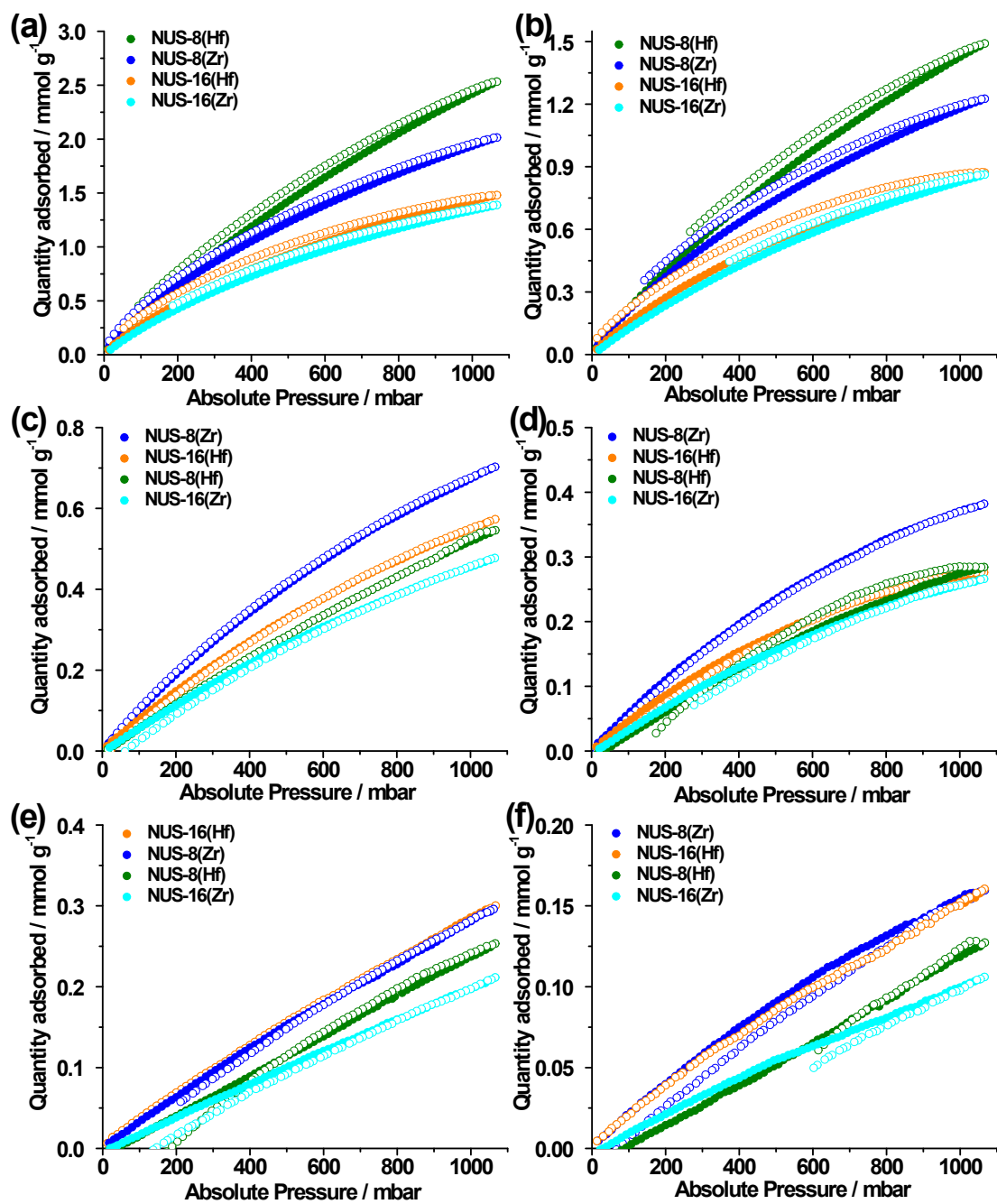


Figure S6. Gas sorption study: CO₂ at 273 K (a) & 298 K (b); N₂ at 273 K (c) & 298 K (d); CH₄ at 273 K (e) & 298 K (f).

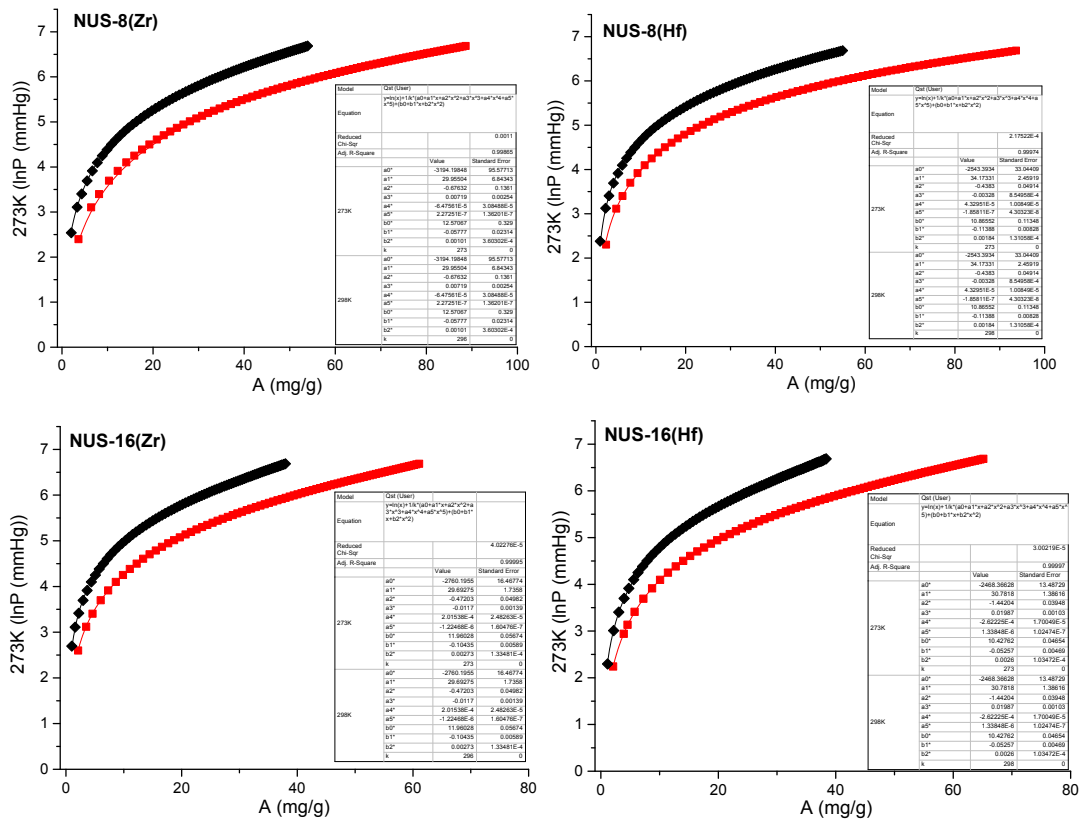


Figure S7. Parameter fittings for the calculation of adsorption heat in NUS-8 and NUS-16.

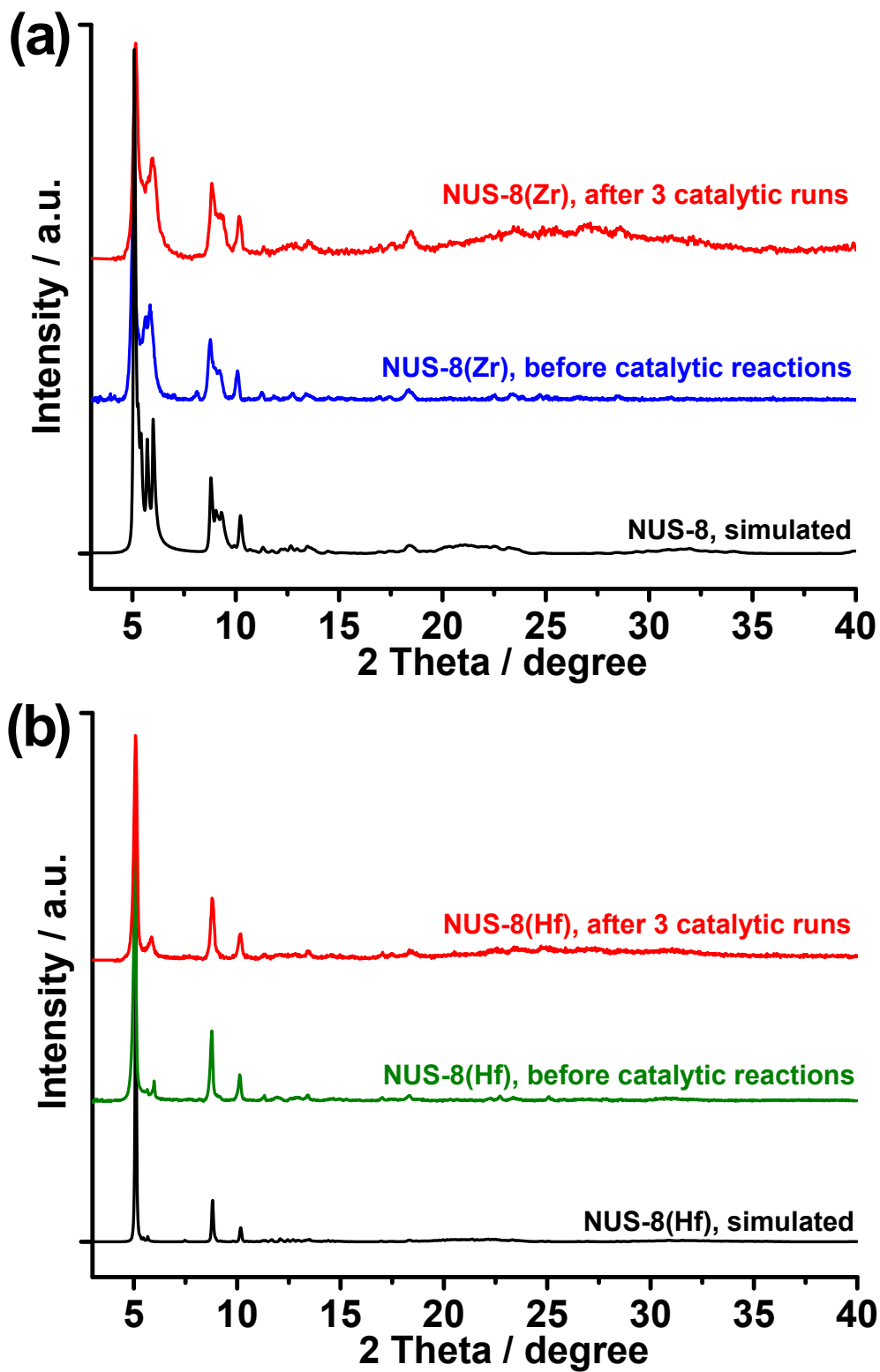


Figure S8. PXRD patterns of NUS-8 before and after three catalytic runs.

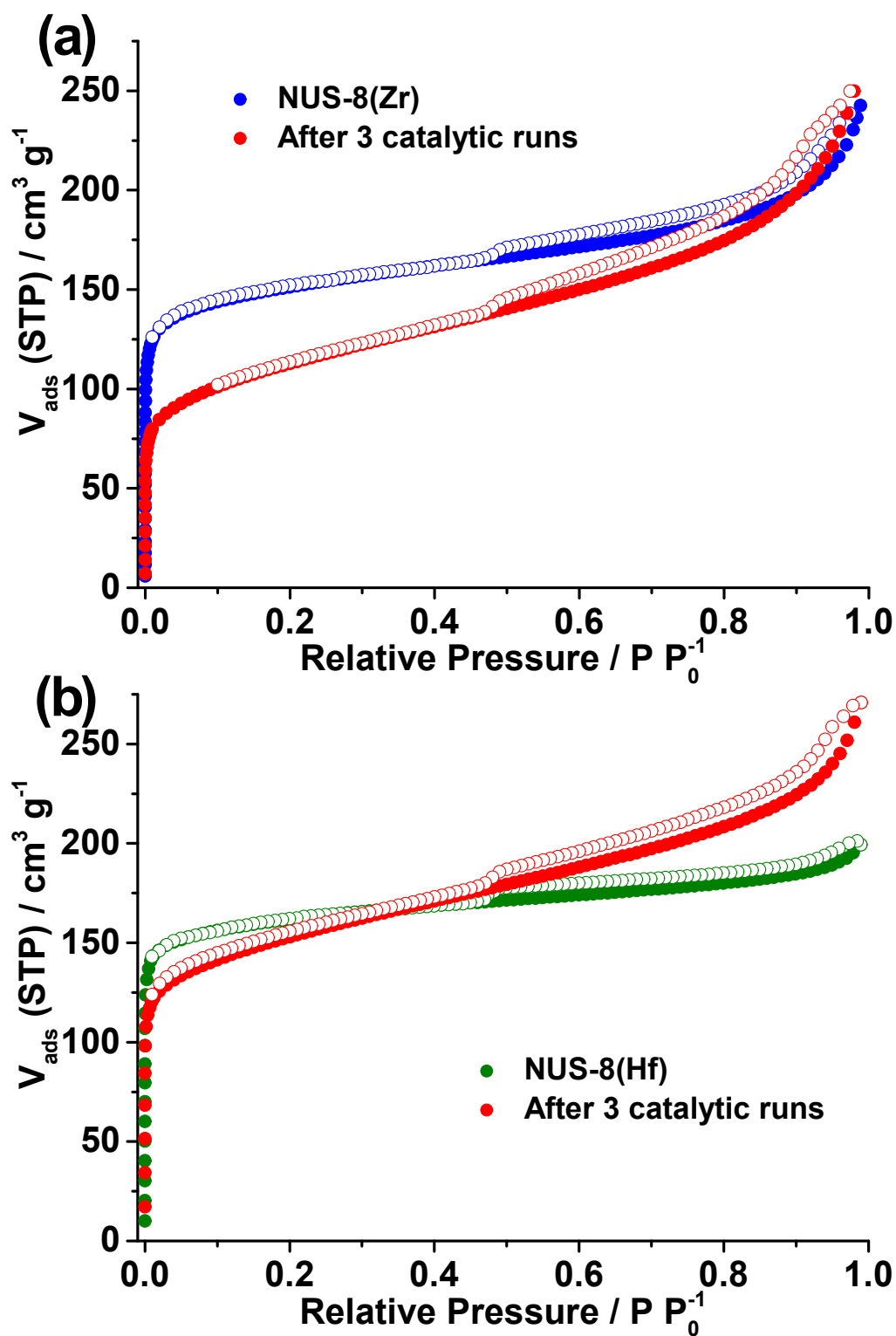


Figure S9. N_2 isotherms at 77K of NUS-8 before and after three catalytic runs.

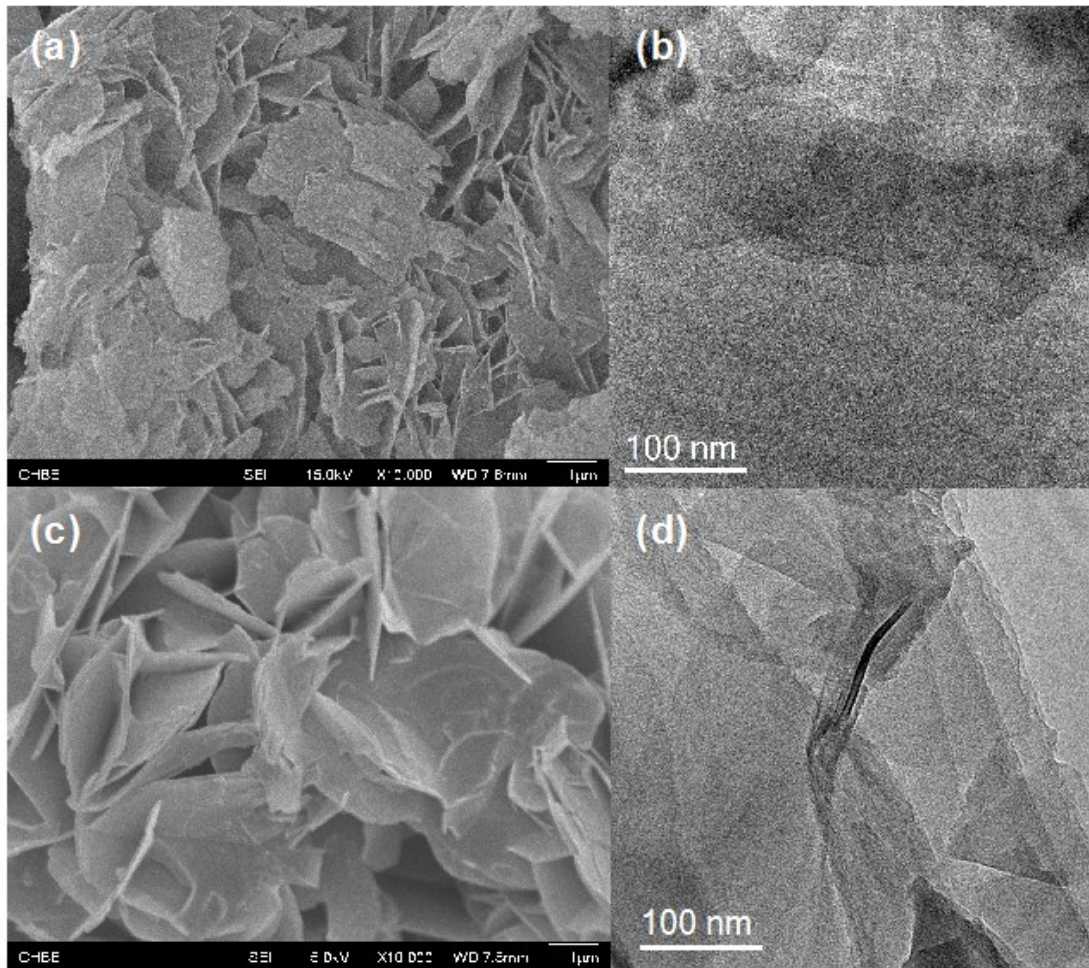


Figure S10. FESEM (a, c) and TEM (b, d) images of NUS-8(Zr) before (a-b) and after (c-d) three catalytic runs.

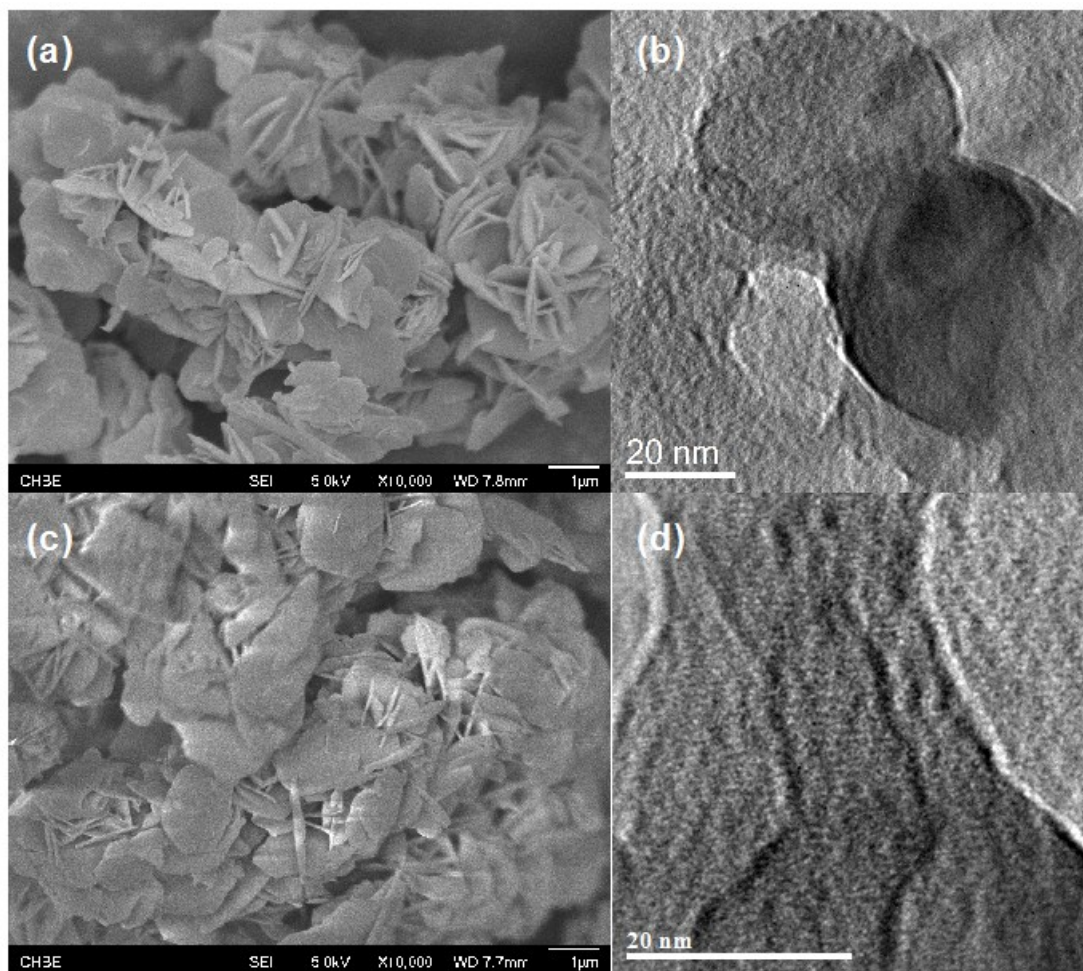


Figure S11. FESEM (a, c) and TEM (b, d) images of NUS-8(Hf) before (a-b) and after (c-d) three catalytic runs.

Table S1. Crystal data and refinement details for NUS-8 MOFs.

Sample	NUS-8(Zr)	NUS-8(Hf)
Temperature (K)	300	300
Wavelength (Å)	0.9998	0.9998
Formula	C ₂₁₆ H ₁₂₀ O ₁₂₈ Zr ₂₄	C ₂₁₆ H ₁₂₀ O ₁₂₈ Hf ₂₄
Formula weight	6980	9068
Crystal system	Monoclinic	Monoclinic
Space group	P2 ₁ /m	P2 ₁ /m
<i>a</i> (Å)	20.0290	20.3601
<i>b</i> (Å)	33.6370	34.5456
<i>c</i> (Å)	18.1820	18.7048
α	90.0000	90.0000
β	112.5840	111.8245
γ	90.0000	90.0000
<i>V</i> (Å ³)	11310.2	12213.1
<i>Z</i>	3	3
<i>D</i> _{calc} (g cm ⁻³)	1.025	1.233
<i>R</i> _{wp}	2.745	1.587
<i>R</i> _p	1.558	1.110
<i>R</i> _{exp}	3.981	3.550
χ^2	0.476	0.200

*R*_{wp}: the weighted profile R-factor calculated for the full pattern; *R*_p: the unweighted profile R-factor calculated for the full pattern; *R*_{exp}: the statistically expected R value; χ^2 : the cumulative value.

Table S2. Surface area (SA), pore volume, and gas uptake of NUS-8 and NUS-16.

		NUS-8(Zr)	NUS-8(Hf)	NUS-16(Zr)	NUS-16(Hf)
BET SA ^{a)}		570	628	592	392
Langmuir SA ^{a)}		643	736	698	469
Pore volume ^{b)}		0.32	0.34	0.33	0.20
CO ₂ uptake at 0.15 bar ^{c)}	298 K	0.30	0.31	0.18	0.22
CO ₂ uptake at 1 bar ^{c)}	298 K	1.18	1.43	0.83	0.85
	273 K	1.94	2.42	1.33	1.42
CH ₄ uptake at 1 bar ^{c)}	298 K	0.37	0.27	0.26	0.27
	273 K	0.67	0.52	0.46	0.55
N ₂ uptake at 1 bar ^{c)}	298 K	0.15	0.12	0.10	0.15
	273 K	0.28	0.24	0.20	0.28

^{a)} m² g⁻¹, ^{b)} cm³ g⁻¹, ^{c)} mmol g⁻¹, ^{d)} cm³ g⁻¹

Table S3. Q_{st} at low coverage and IAST adsorption selectivity of NUS-8 and NUS-16 MOFs.

	NUS-8(Zr)	NUS-8(Hf)	NUS-16(Zr)	NUS-16(Hf)
Q_{st} of CO ₂ ^{a)}	26.5	21.2	23.0	20.5
Q_{st} of CH ₄ ^{a)}	18.5	17.5	16.8	16.5
Q_{st} of N ₂ ^{a)}	14.0	11.5	12.6	12.3
IAST selectivity: CO ₂ /N ₂ ^{b)}	14	11	12	9
IAST selectivity: CO ₂ /CH ₄ ^{c)}	5.6	3.9	4.2	3.2

^{a)} kJ mol⁻¹, absolute value, ^{b)} CO₂:N₂ = 15:85, 298 K 1 bar. ^{c)} CO₂:CH₄ = 50:50, 298 K 1 bar.

Table S4. Elementary analysis (EA) and thermogravimetric analysis (TGA) results of NUS-8.

Weight%	NUS-8(Zr)		NUS-8(Hf)	
	Before	After ^a	Before	After ^a
C	36.85 (37.13 ^b)	37.15	27.96 (28.58 ^b)	29.15
H	1.85 (1.83 ^b)	1.74	1.24 (1.32 ^b)	1.15
M (Zr or Hf)	32.21 (31.29 ^b)	31.15	47.36 (47.11 ^b)	47.23
M/C weight ratio	0.87 (0.84 ^b)	0.83	1.65 (0.84 ^b)	1.62
Ligand to metal cluster molar ratio ^c	1.852 (2 ^b)	N.A.	1.932 (2 ^b)	N.A.

^a after 3 catalytic runs; ^b calculated from crystal model; ^c from the TGA results; N.A.: not applied.

References

- (1) Hu, Z.; Peng, Y.; Kang, Z.; Qian, Y.; Zhao, D. A Modulated Hydrothermal (MHT) Approach for the Facile Synthesis of UiO-66-Type MOFs. *Inorg. Chem.* **2015**, *54*, 4862-4868.
- (2) Hu, Z.; Nalaparaju, A.; Peng, Y.; Jiang, J.; Zhao, D. Modulated Hydrothermal Synthesis of UiO-66(Hf)-Type Metal–Organic Frameworks for Optimal Carbon Dioxide Separation. *Inorg. Chem.* **2016**, *55*, 1134–1141.
- (3) Wang, R.; Wang, Z.; Xu, Y.; Dai, F.; Zhang, L.; Sun, D. Porous Zirconium Metal – Organic Framework Constructed from 2D → 3D Interpenetration Based on a 3,6-Connected kgd Net. *Inorg. Chem.* **2014**, *53*, 7086-7088.
- (4) Altomare, A.; Cuocci, C.; Giacobozzo, C.; Moliterni, A.; Rizzi, R.; Corriero, N.; Falcicchio, A. EXPO2013: a kit of tools for phasing crystal structures from powder data. *J. Appl. Crystallogr.* **2013**, *46*, 1231-1235.
- (5) Jiang, J.; Yaghi, O. M. Brønsted Acidity in Metal–Organic Frameworks. *Chem. Rev.* **2015**, *115*, 6966-6997.
- (6) Dincă, M.; Long, J. R. Hydrogen Storage in Microporous Metal-Organic Frameworks with Exposed Metal Sites. *Angew. Chem., Int. Ed.* **2008**, *47*, 6766-6779.
- (7) Myers, A. L.; Prausnitz, J. M. Thermodynamics of mixed-gas adsorption. *AIChE J.* **1965**, *11*, 121-127.
- (8) Kholdeeva, O. A.; Maksimov, G. M.; Maksimovskaya, R. I.; Kovaleva, L. A.; Fedotov, M. A.; Grigoriev, V. A.; Hill, C. L. A Dimeric Titanium-Containing Polyoxometalate. Synthesis, Characterization, and Catalysis of H₂O₂-Based Thioether Oxidation. *Inorg. Chem.* **2000**, *39*, 3828-3837.
- (9) Huang, L.; Wang, S.-S.; Zhao, J.-W.; Cheng, L.; Yang, G.-Y. Synergistic Combination of Multi-ZrIV Cations and Lacunary Keggin Germanotungstates Leading to a Gigantic Zr₂₄-Cluster-Substituted Polyoxometalate. *J. Am. Chem. Soc.* **2014**, *136*, 7637-7642.
- (10) Mahdi, E. M.; Tan, J.-C. Dynamic molecular interactions between polyurethane and ZIF-8 in a polymer-MOF nanocomposite: Microstructural, thermo-mechanical and viscoelastic effects. *Polymer* **2016**, *97*, 31-43.
- (11) Mahdi, E. M.; Tan, J.-C. Mixed-matrix membranes of zeolitic imidazolate framework (ZIF-8)/Matrimid nanocomposite: Thermo-mechanical stability and viscoelasticity underpinning membrane separation performance. *J. Membr. Sci.* **2016**, *498*, 276-290.